The Astrophysical Journal, 820:75 (14pp), 2016 March 20 doi:10.3847/0004-637X/820/1/75

LINE IDENTIFICATIONS OF TYPE I SUPERNOVAE: ON THE DETECTION OF Si II FOR THESE HYDROGEN-POOR EVENTS

J. T. Parrent[1], D. Milisavljevic[1], A. M. Soderberg[1], and M. Parthasarathy[2]
[1] Harvard-Smithsonian Center for Astrophysics, 60 Garden Street, Cambridge, MA 02138, USA
[2] Indian Institute of Astrophysics, Koramangala, Bangalore, 560034, India
Received 2015 May 3; accepted 2016 February 4; published 2016 March 21

ABSTRACT

Here we revisit line identifications of type I supernovae (SNe I) and highlight trace amounts of unburned hydrogen as an important free parameter for the composition of the progenitor. Most one-dimensional stripped-envelope models of supernovae indicate that observed features near 6000–6400 Å in type I spectra are due to more than Si II λ6355. However, while an interpretation of conspicuous Si II λ6355 can approximate 6150 Å absorption features for all SNe Ia during the first month of free expansion, similar identifications applied to 6250 Å features of SNe Ib and Ic have not been as successful. When the corresponding synthetic spectra are compared with high-quality timeseries observations, the computed spectra are frequently too blue in wavelength. Some improvement can be achieved with Fe II lines that contribute redward of 6150 Å; however, the computed spectra either remain too blue or the spectrum only reaches a fair agreement when the rise-time to peak brightness of the model conflicts with observations by a factor of two. This degree of disagreement brings into question the proposed explosion scenario. Similarly, a detection of strong Si II λ6355 in the spectra of broadlined Ic and super-luminous events of type I/R is less convincing despite numerous model spectra used to show otherwise. Alternatively, we suggest 6000–6400 Å features are possibly influenced by either trace amounts of hydrogen or blueshifted absorption and emission in Hα, the latter being an effect which is frequently observed in the spectra of hydrogen-rich, SNe II.

Key words: supernovae: general

1. INTRODUCTION

Studying the evolution of a supernova's spectral energy distribution is a formidable task on account of excessive line blending that for all intents and purposes erases most traces of a reference continuum level. Specific line transitions that contribute to conspicuous features in SN Ia spectra have been mostly identified, whereas the identification of weak spectral features for most SN I supernovae remain uncertain (see Table 1). Line blending on the scale generated by the large expansion velocities ($>10^4$ km s^{-1}) thus creates a number of hurdles for supernova spectroscopists who are interested in extracting information about the composition of the ejecta (cf. Gaposchkin 1936; Popper 1937).

In terms of a taxonomy or a observed spectral sequence, supernovae of various luminosity classes are divided into two central categories: type I and type II, depending on whether the spectrum contains conspicuous signatures of hydrogen (Minkowski 1941). For type II supernovae (SNe II), signatures of hydrogen Balmer lines come in the form of distinct P Cygni profiles. Depending on the decline in the light curve, SNe II can be further subclassified as SN IIL for a linear decline and SN IIP for sustained brightness before an eventual decline. However, drawing distinctions between SN IIL and IIP is less obvious considering an existing continuum of observed properties (Faran et al. 2014; Sanders et al. 2015; Chakraborti et al. 2016; Gall et al. 2015; Pejcha & Prieto 2015).

Broadly speaking, hydrogen-poor SN I supernovae can be separated into three subclasses: SN Ia, Ib, and Ic. In addition, the spectra of SN IIb evolve from SN II in appearance with weak Hα, but later transition to a spectrum with lines of helium similar to SN Ib (Filippenko 1988). Due to similarities between some caught-early SN Ib to SN IIb at later times, some SN Ib may be caught-late SN IIb (Folatelli et al. 2014; see also Liu et al. 2015).

Types Ib and Ic are generally distinguished by the presence or absence of obvious helium signatures (Wheeler et al. 1995; Dessart et al. 2015b). Additionally, thermonuclear SN Ia reveal conspicuous signatures of Si II λ6355, while the latter varieties of SN I core-collapse supernovae do not (Filippenko 1997); i.e., stripped-envelope subclasses of SN Ib/Ic are defined by Filippenko (1997) and previous authors as not having a conspicuous doublet signature of Si II λ6355, which is a line detected for all SN Ia (Wheeler et al. 1995).

For a comparison of these types of supernovae, in Figure 1 we plot the SN Ib 1984L, SN IIpec 1987A, SN Ic 1987M, and SN Ia 2011fe and note the similarity of 6250 Å features between SN II-peculiar 1987A and SN Ic 1987M is striking. However, in the similar Figure 1 of Filippenko (1997), weak absorption features near 6250 Å are labeled as Si II for both "SN Ib" 1984L and "SN Ic" 1987M, implying the spectra harbor a lone and weak feature of silicon when this feature may instead be influenced by trace amounts of hydrogen for some SN Ib (James & Baron 2010).

A precise definition of SN Ib/Ic has since varied over the years (see Fryer 2004; Gray & Corbally 2009). Some interpretations assume hydrogen is absent for SN I "by definition of being type I" (cf. Maguire et al. 2010; Eldridge et al. 2013), while lone detections of Si II λ6355 are deemed robust for SN Ib/Ic and therefore accurate for measurement (see, e.g., Taubenberger et al. 2006; Modjaz et al. 2014). Line identifications for 6000−6400 Å features in the spectra of broadlined SN Ic (BL-Ic) and type I/R super-luminous supernovae (SLSNe) have also been debated. Most notably, estimates of Si II and Fe II conflict when 6000–6400 Å spectral features are interpreted to be dominated by Si II, while model spectra producing mostly signatures of Si II are consistently too blue in wavelength when compared with observations (cf. Mazzali et al. 2000; Inserra et al. 2013; Lyman et al. 2016).

Table 1
Common Lines in Optical Spectra of SNe I

Ion	Rest Wavelength (Å)
[a]C II[bc]	6580, 7234
[a]O I[bc]	7774, 8446, 9264
[a]Mg II[bc]	4481, 7896
[a]Ca II[bc]	3969, 3934, 8498, 8542, 8662
[a]Si II	3838, 4130, 5051, 5972, 6355[a]
[a]Si III	4560, 5743
[a]S II	4163, 5032, 5208, 5468, 5654, 6305
[a]Fe II[bc]	4025, 4549, 4924, 5018, 5169
[a]Fe III	4420, 5156, 6000

Notes. If *a* is on the left, an ion has been detected for SN Ia; if *bc* is on the right, an ion has been detected for SN Ib and Ic. Fe III may or may not be detectable if present on account of severe line blending for all SN Ib and Ic. For fast-evolving events, such as SN 2005hk and 2010X, an identification of Si II λ6355 also seems likely (Drout et al. 2013).
[a] When Si II is identified in the spectra of SN Ib, Ic, BL-Ic, and SLSN, it is based on a single line, λ6355, i.e., unconfirmed in the same sense as for Hα.

The case for detectable hydrogen in the SN Ic 1994I was discussed by Wheeler et al. (1994), while Clocchiatti et al. (1996) claimed detections of weak lines of He I as well. Both interpretations were later favored by Parrent et al. (2007) who used SYNOW to show that a mix of both photospheric and higher velocity H I λ6563 offer better alternatives to the unmatched models of Branch et al. (2006) and Sauer et al. (2006), both of which produce strong signatures of Si II. The feature nearest to 6250 Å has also been proposed to be a composite of C II, Ne I, and Si II (Hachinger et al. 2012). However, the abundance of Ne I needed to match observations is reportedly too high to be physically consistent with the final abundances of candidate progenitor systems (Ketchum et al. 2008).

Dessart et al. (2015b) recently produced non-LTE spectrum synthesis calculations stemming from "hydrogen-poor" ($M_{\rm H} \sim 10^{-3}$–$10^{-2}\ M_{\odot}$) and "hydrogen-depleted" models ($M_{\rm H} \sim 10^{-6}\ M_{\odot}$), and have shown that a Si II/Fe II-weighted prescription for 6250 Å features of SN Ib/Ic may provide a more plausible alternative to treating weak signatures of Hα as a free parameter. These models also indicate that if the progenitor star has above $10^{-3}\ M_{\odot}$ of hydrogen within a thin shell on its surface (i.e., not physically detached), then the corresponding post-explosion Hα profile near 6250 Å will resemble that of SN IIb so long as the surface abundance of hydrogen is high enough. However, the rise-time of these SN Ib and SN Ic models is roughly twice as long as what is typically observed (cf. Wheeler et al. 2015), which questions the model's ability to represent "standard compositions."

Finally, recent observations of the SN Ib 2014C reveal evidence for interaction with a hydrogen-rich circumstellar medium (CSM) that was expelled in the years prior to the explosion (Milisavljevic et al. 2015; see also Chugai & Chevalier 2006; Moriya et al. 2015; Yan et al. 2015). Should we then expect trace amounts of hydrogen to remain within the outermost layers of the progenitor for some of these type I core-collapse events?

In this work we examine the latest model spectra for SNe I and confront them with observations. In Section 2 we highlight some current pitfalls when invoking detections and non-detections of select atomic species. In Section 3 we give an overview of the ability of various explosion models to reproduce 6000−6400 Å features in the spectra of SN Ia, Ib, Ic, and more luminous events. In Section 4 we summarize our findings.

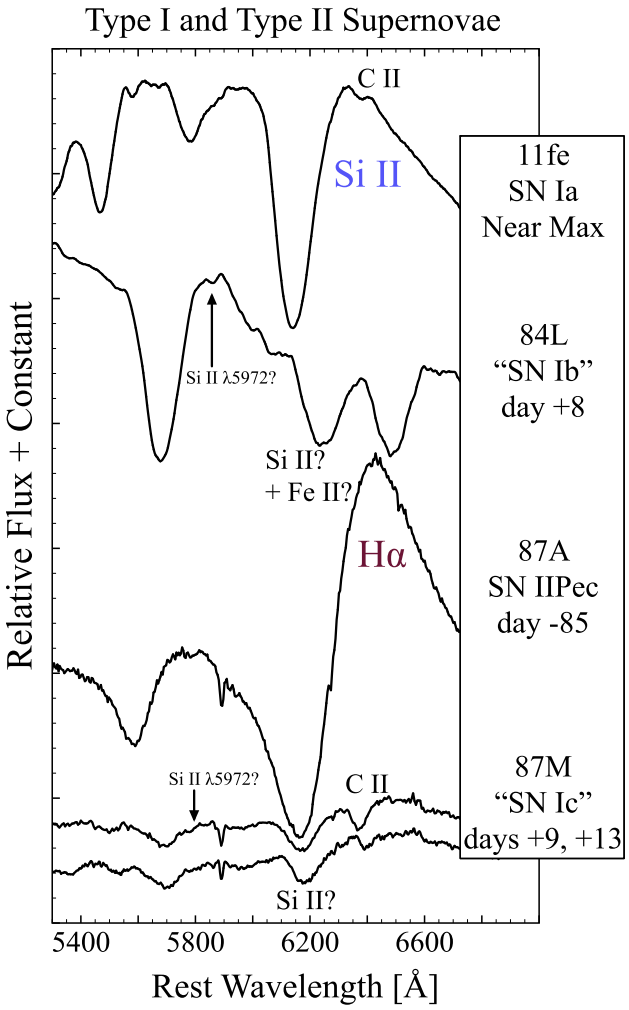

Figure 1. Comparisons of spectra from SN 1987A soon after the explosion on UT 1987 February 24 (Pun et al. 1995); SN 1984L at approximately day +8 relative to *B*-band maximum light (Doggett & Branch 1985; Wheeler & Levreault 1985; Tsvetkov 1987); SN 1987M on UT 1987 September 28 and UT 1987 October 2, approximately days +9 and +13, respectively, relative to *B*-band maximum light (Filippenko et al. 1990; Jeffery et al. 1991); and SN 2011fe near maximum light (Pereira et al. 2013). Labels for SN 1987A and 2011fe denote ions for which detections have been verified, while labels for the 6250 Å features of SN 1984L and 1987M represent unproven candidate ions. For SN 2011fe, 1984L, and 1987A a single epoch is shown, whereas for SN 1987M two epochs are shown (+9, +13).

2. SPECTRAL LINE IDENTIFICATION

Line blending is so severe for supernova spectra that it permits broad consistency between a synthesized spectrum and a majority of observed spectral features. These include absorption and emission line signatures that can be either conspicuous or weak below limiting noise. Some of these features can be approximated to a few lines, while others sustain a complex blend from first light to well after a year of the explosion.

Whether testing a benchmark model or tracing observed features with a prescription of candidate lines, the interpretation of the observed spectral features and the related empirical

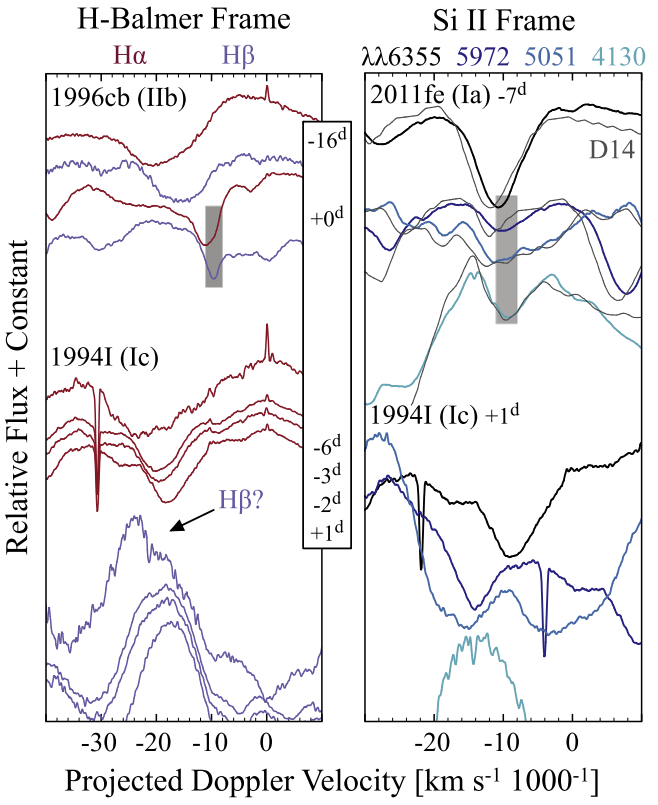

Figure 2. Plotted above are the projected Doppler velocities $\mathcal{O}(v/c)$ in the frame of the strongest H-Balmer lines (left) and Si II lines (right). The light gray bands are meant to indicate the overlap between common signatures of a given ion. Spectrum references: SN 1994I (Modjaz et al. 2014); SN 1996cb (Matheson et al. 2001); and SN 2011fe (Pereira et al. 2013). Model references: (D14) PDDEL4, day −6.6 for SN 2011fe by Dessart et al. (2014a).

measurements depend on the quality of the full fit from the supporting model. Moreover, if a model spectrum produces all but a single (or few) observed feature(s), the model is judged to be significantly incomplete. The same is true if the model produces spectral signatures that are not observed at the same epoch of the observation. Considering the relationships between the composition of the ejecta and the energy throughout, when a model's light curves are in good agreement with observations, the model spectra must also reflect observations before a model is sufficiently matched, and vice versa.

Since boundaries between spectral line signatures are not well-defined for most supernovae, empirical false positives are readily available within an underspecified parameter space of "detections." Consequently, detections and non-detections of various ions and spectral lines do not follow classical definitions. For example, a non-detection of the strongest line from an ion at 5500 Å does not necessarily imply a lack of significant spectral contamination from either this or other ions at 5500 Å and other wavelengths. This can be made worse by low signal-to-noise ratio data and inadequate spectroscopic follow-up.

A common example is singly ionized silicon. This ion is considered detected in SN Ia optical spectra when a number of spectral lines are conspicuous above noise and additional blending from adjacent lines. However, additional signatures of Si II $\lambda\lambda$3858, 5972 are not definitively detected for SN Ib, Ic, and SLSN I.

See Figure 2 where we have plotted photospheric phase spectra of the SN Ia 2011fe (Pereira et al. 2013) and the SN Ic 1994I (Filippenko et al. 1995) in terms of Si II and H I line velocities $\mathcal{O}(v/c)$. For SN 2011fe, its spectra are reasonably influenced by the so-called conspicuous lines of Si II. In comparison with SN Ib/Ic, a lack of obvious Si II λ5972 is to be expected since the stronger Si II λ6355 would already be a weak signature compared with that for SN Ia; i.e., a purported identification of Si II λ6355 so far has only one wavelength region by which to constrain the associated model.

Other ions with few strong lines, such as H I, C II, C III, Na I, and Si IV, face similar obstacles during photospheric phases as well, while a signature of Na I D is arguably absent for SN Ia, minimal or absent for SN Ib, and significantly present for SN Ic (Dessart et al. 2012, 2014b, 2015b). Hence, studies of ejecta compositions benefit when the number of candidate lines is either effectively maximized or close to the number of lines that are suspected to be present (Baron et al. 1996; Friesen et al. 2014; Vacca et al. 2015).

These are important points to consider when interpreting type I spectra, given that freshly synthesized ejecta are potentially contaminated by unburned and distinguishable traces of H, He, C, O, Si, Ca, and Fe-rich progenitor material near and above the primary volume of line formation (a so-called "photosphere," see Hatano et al. 1999; Branch et al. 2005). Additionally, an observed spectral signature associated with a particular ion at photospheric velocities can be influenced by an identical ion in addition to other atomic species at similar or relatively higher velocities (Marion et al. 2013) (see Figure 3 of Blondin et al. 2015).

For example, Sasdelli et al. (2014) claim non-detections for all signatures of carbon in the early spectra of the peculiar SN Ia 1991T without providing an explanation for a tentative detection of C III λ4649. This identification is also consistent with kinetic energies deduced from detectable lines of Fe III and a tentative detection of Si III. For the computed spectrum at 4500 Å, a feature is missing exactly where it is present for SN 1991T, 1997br, and 1999aa during early pre-maximum epochs. Therefore, abundance determinations of unburned carbon would benefit from knowing the subset of species giving rise to weak 4500 Å features in the spectra of SN 1991T/1999aa-like events (Hatano et al. 2002; Parrent et al. 2011, 2014).

Detections of select atomic species are most apparent when line-blanketing effects are strong. A classic example is the absorption trough of Ti II observed for SN 1991bg and 1999 by on account of overall lower ejecta temperatures (Doull & Baron 2011 and references therein). By contrast, less conspicuous detections of Ti II will be blended and relatively ambiguous against a backdrop of signatures from other iron-peak elements. This is the root of the problem when subclassifying supernovae according to their spectral features.

As an example, White et al. (2015) utilize non-detections of the Ti II absorption trough observed blueward of 4450 Å in an effort to distinguish peculiar SN 2002es-likes with conspicuous Ti II (Ganeshalingam et al. 2012) from SN 2002cx-likes found without the classically seen trough of Ti II absorption (Li et al. 2003). It is important to note, however, that despite claims of non-detections of Ti II, the ejecta and spectra of SN 2002cx-likes are not likely void of Ti II (see Foley et al. 2009; Kromer et al. 2013; Stritzinger et al. 2014).

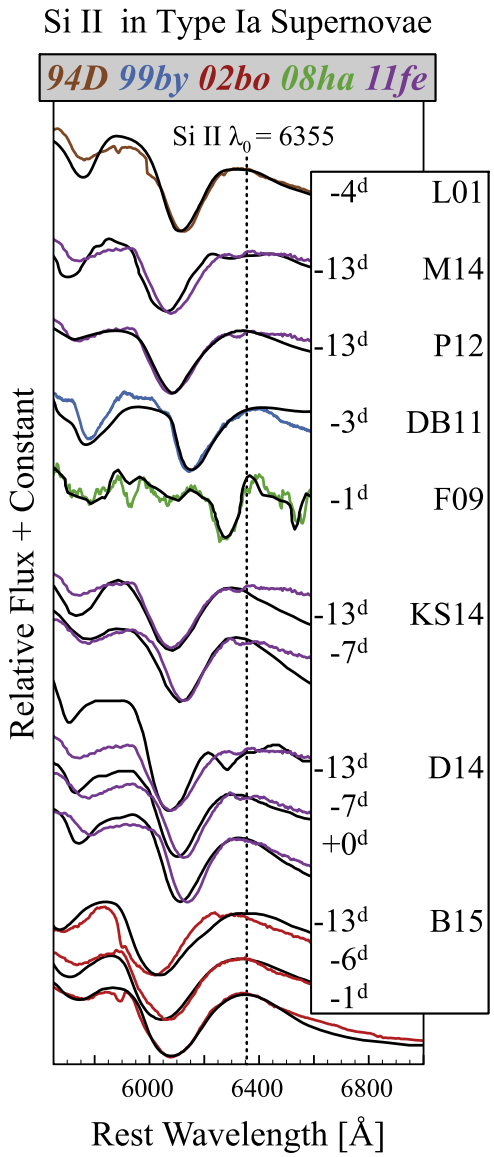

Figure 3. Comparisons between computed and observed spectra of select SN Ia. Spectrum references: SN 1994D (brown), Patat et al. (1996); SN 1999by (blue), Garnavich et al. (2004); SN 2002bo (red), Benetti et al. (2004); SN 2008ha (green), Foley et al. (2009); SN 2011fe (purple), Parrent et al. (2012), Pereira et al. (2013), and Mazzali et al. (2014). Model references: (L01) Lentz et al. (2001); (M14) Mazzali et al. (2014); (P12) Parrent et al. (2012); (DB11) Doull & Baron (2011); (F09) Foley et al. (2009); (KS14) Kerzendorf & Sim (2014); (D14) Dessart et al. (2014a); and (B15) Blondin et al. (2015).

3. MODEL SPECTRA OF SNE I NEAR 6000–6400 Å

In this section we examine SN I synthetic spectra found throughout the literature and assess respective goodness-of-fits when compared with observations. For each model spectrum shown, we have attempted to preserve the flux scaling for comparisons between observed and synthesized data in the original works, and we have normalized the spectra with respect to the 6000−6400 Å profiles where appropriate. (This underscores the need for releasing all published model spectra and photometry.)

3.1. Thermonuclear SN Ia

Plotted in Figure 3 are observations of SN Ia subtypes compared with the computed spectra from various spectrum synthesizers at wavelengths spanning 5200–7000 Å. All model spectra, generated from semi-empirical to full non-LTE radiation transport solvers, are capable of providing a close match to the feature centered about 6150 Å through prescriptions based on Si II λ6355.

Specifically, all absorption and emission components are well-centered with the data, while the curvature of the profile wings are relatively well-matched. This is also in spite of either a "non-standard" distribution of Si II, or two distinct components of photospheric and detached Si II λ6355. That is, precise and accurate predictions are achievable for the red and blue wings, which are both sensitive to mean expansion velocities and the radial decline in density.

To further appreciate the limiting accuracy of 6150 Å features in SN Ia spectra as having been identified as Si II λ6355, consider that an intrinsic difference of 500, 1000, and 2000 km s^{-1} in terms of line velocities would be reflected by an underlying shift of ∼10, 20, and 40 Å, respectively. That is, apart from opacity effects, significant differences of 2000 km s^{-1} can give rise to 40 Å blue-shifts that are of similar order to redshifts seen for 6150 Å features during the first month of free expansion. Despite these differences, model spectra for SN Ia consistently reflect a suite of observations.

When confronted by events such as the SN Ia 2012fr (Childress et al. 2013; Maund et al. 2013), where the conspicuousness of a higher velocity signature of Si II λ6355 is sensitive to the cadence of follow-up observations, approximate consistency with composite features near 6150 Å is relatively large for SN Ia. In other words, the relative location of high velocity Si II would not be well-constrained without the accompanying timeseries spectra. As we will discuss in Section 3.4, this window of consistency is even greater for broadlined SN Ic (BL-Ic) and SLSN.

One reason a model SN Ia might not match near the emission component of the Si II is when the model does not center C II λ6580 at similar projected Doppler velocities as Si II during the first month after the explosion (Taubenberger et al. 2011; Pereira et al. 2013). Other lines that impact this region for SN Ia include S II λ6305 and lines of Fe II near maximum light and thereafter. Despite these additional biases on direct measures of Si II features, the identification of Si II λ6355 as a dominant line in the spectra of SN Ia is robust for a variety of normal and peculiar events.

3.2. Core-collapse Supernovae

Based on the recent spectrum synthesis calculations from Dessart et al. (2015b) who utilize a modified version of CMFGEN (Hillier & Dessart 2012), stripped-envelope models that produce weak signatures of Si II λ6355 may avoid both consistent mismatch and the need for trace hydrogen by relying on contribution from Fe II as well as He I in some instances (Dessart et al. 2012). In this case, Fe II effectively moves a signature dominated by Si II toward redder wavelengths, thereby making a blend of Si II and Fe II a strong contender for 6250 Å features of SN Ib/Ic spectra.

Dessart et al. (2015b) also draw associations with the observed spectral sequence of SN IIb, Ib, and Ic, but without comparing any of these models with observations. Notably, the SN Ib 6p5Ax1 model of Dessart et al. (2015b) has a rise-time of 40 days. This rise-time is nearly twice as long as those typically observed for SN Ib, while the SN Ic 5p11Ax1 from Dessart et al. (2015b) has a rise-time that conflicts with most

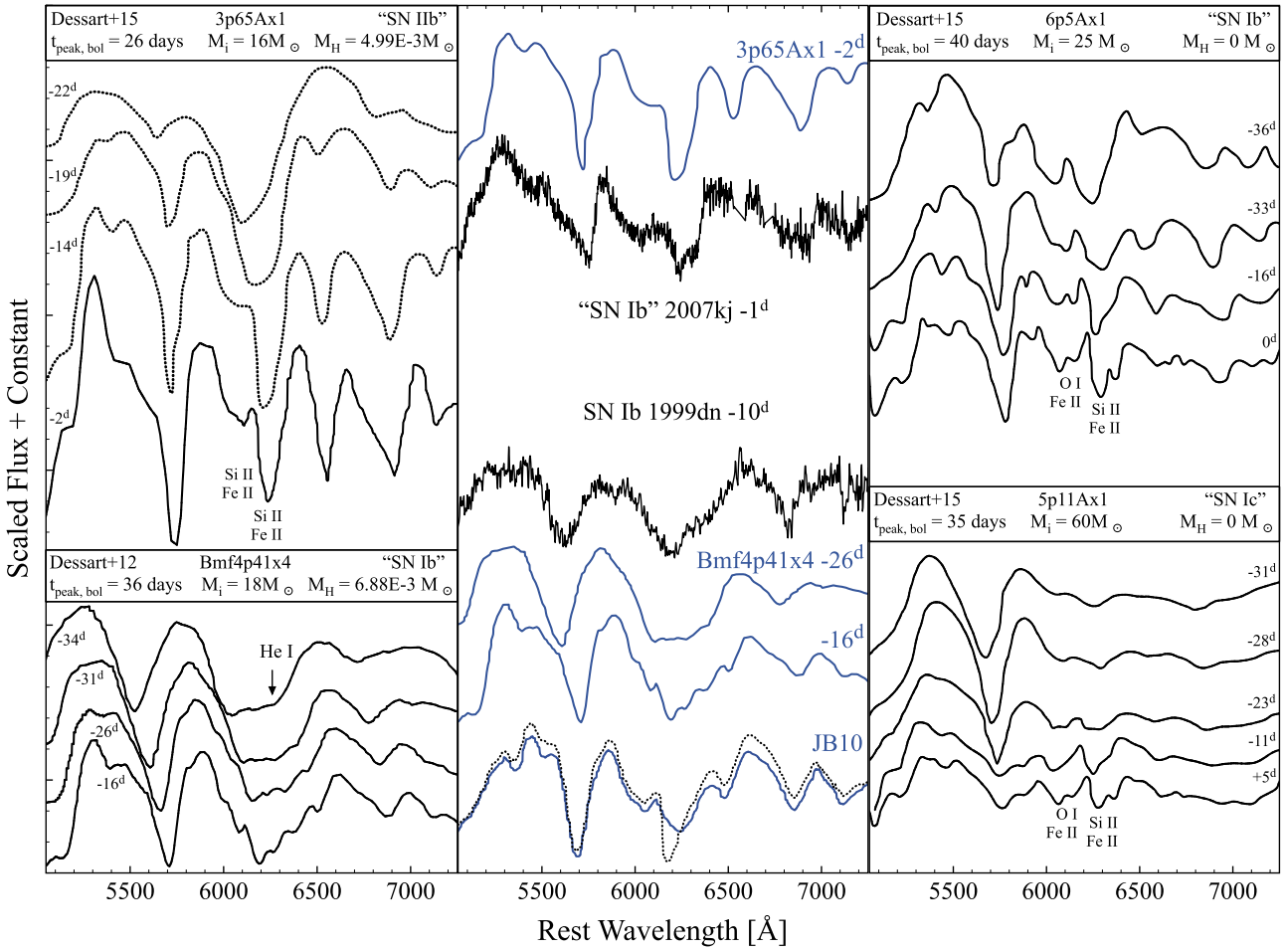

Figure 4. Comparisons between computed spectra, SN 2007kj (Modjaz et al. 2014), and SN 1999dn (Deng et al. 2000). The data have been scaled and normalized according to Jeffery et al. (2007). In the four corner panels we plot timeseries spectra of the SN IIb 3p65Ax1, SN Ib 6p5Ax1, and SN Ic 5p11Ax1 models presented by Dessart et al. (2015b) and also include the earliest spectra of the "standard SN Ib" Bmf4p41x4 presented by Dessart et al. (2012). The rise-time, initial mass, and final hydrogen mass for each model is listed in each panel. Dotted lines denote when the spectrum is contaminated by signatures of Hα. Certain features are labeled by ions producing significant structure within the computed spectrum. JB10 PHOENIX calculation of James & Baron (2010) with and without hydrogen are shown as the dashed black line and the solid blue line, respectively.

observations as well (cf. Wheeler et al. 2015). The "Bmf5p09" series of models presented by Dessart et al. (2012) also exhibit rise-times that conflict with observations by as much as 30 days.

Since the modified version of CMFGEN that is used for supernovae has not been made publicly available, we are unable to test areas of improvement for any of the proposed models. The model spectra from Dessart et al. (2012, 2015) have also not been made available for comparative studies, which was done for the SN Ia models computed by Blondin et al. (2015). Therefore, we take the liberty of digitizing model spectra of interest to plot them against the observations in Figures 4–7.

3.2.1. "SN Ib" 2007kj

In an effort to distinguish SN IIb, Ib, and Ic from their spectra, Liu et al. (2015) recently conducted a comparative study of "the largest spectroscopic data set" of stripped-envelope supernovae. Using the Supernova Identification tool, SNID (Blondin & Tonry 2007), and pseudo equivalent measurements of several spectral features, Liu et al. 2015 classify SN 2007kj as a SN Ib. Modjaz et al. (2014) previously used SNID to classify SN 2007kj as a SN Ib as well.

However, comparison with the SN IIb 3p65Ax1 model spectrum presented by Dessart et al. (2015b), plotted in our Figure 4, would imply that SN 2007kj is instead either a caught-late or slow-evolving SN IIb. That is, in spite of having incorporated the largest set of SNID templates to classify SN IIb, Ib, and Ic, Modjaz et al. (2014), and Liu et al. (2015) are unable to type SN 2007kj as a SN IIb.

Furthermore, if the SN IIb 3p65Ax1 model had been built for SN 2007kj, the match to SN 2007kj would suggest the progenitor had $\sim 10^{-3}$–10^{-2} $M_{\odot}$ of hydrogen on its surface at the time of explosion. It is also important to note that the 6250 Å feature for the day −2 spectrum for the SN IIb 3p65Ax1 model is not contaminated by Hα. This is in spite of a similar 6250 Å feature on day −14 (and earlier) where an Hα signature is present for the model. By maximum light, this feature is predicted to be dominated by profiles of Si II and Fe II (Baron et al. 1995; Dessart et al. 2015b).

3.2.2. SN Ib 1999dn

The computed spectra of the SN Ib Bmf4p41x4 model are also associated with a progenitor having $\sim 10^{-3}$ $M_{\odot}$ of hydrogen near its surface (Dessart et al. 2012). See the bottom

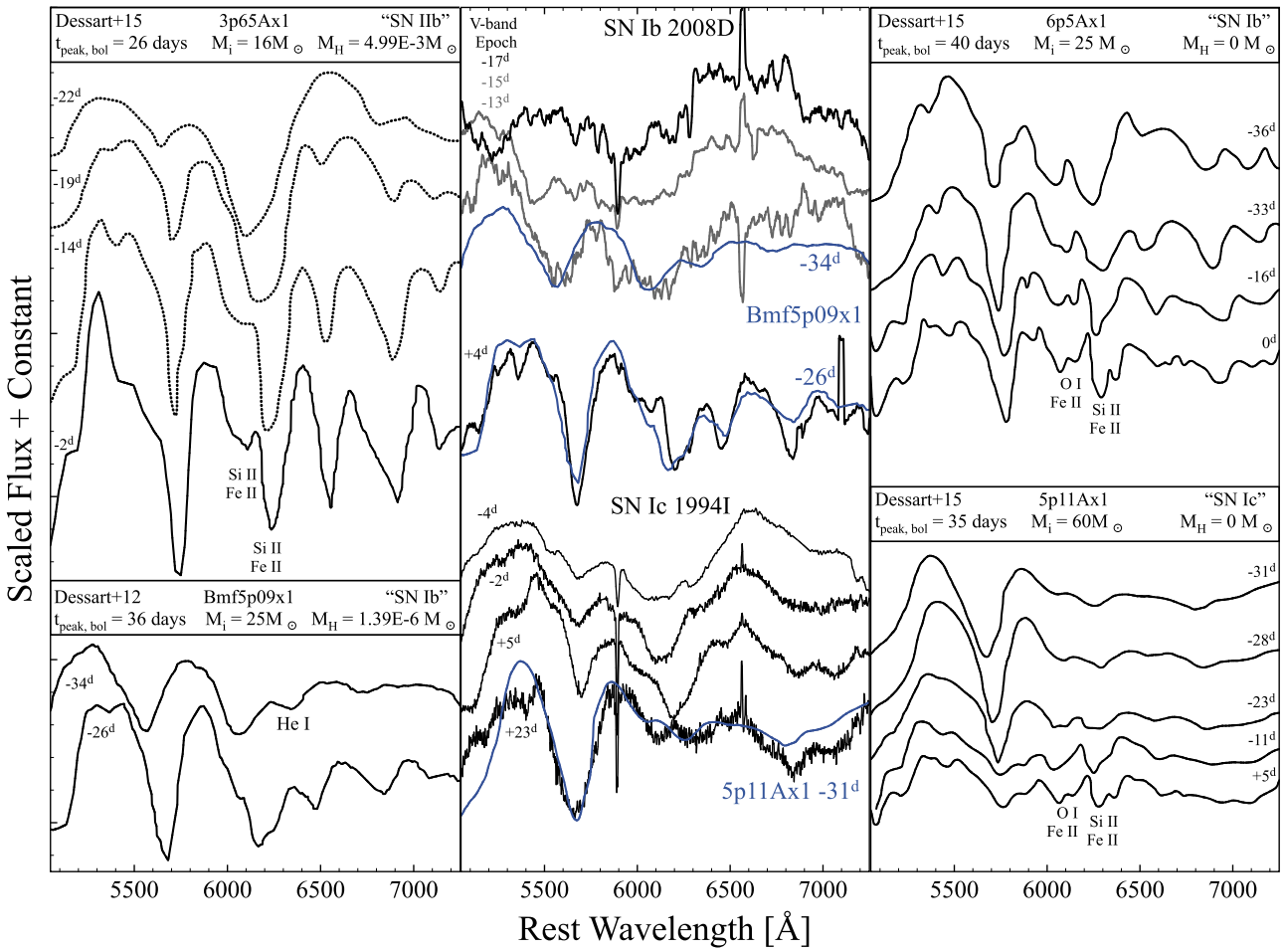

Figure 5. Same as Figure 4 except now for SN 2008D (Soderberg et al. 2008; Modjaz et al. 2009) and SN 1994I (Modjaz et al. 2014). We have replaced the Bmf4p41x4 spectra with those of Bmf5p09x1 from Dessart et al. (2012).

left panel of our Figures 4 and 7. The difference to note between the day −2 spectrum of the aforementioned SN IIb 3p65Ax1 and SN Ib Bmf4p41x4 models is that the shape of the 6250 Å feature in the latter is not SN II-like nor is its spectrum "Hα-positive." This is in spite of the hydrogen present in the ejecta, while the 6250 Å feature is also blended with He I.

Looking at the middle panel of Figure 4, we find a promising match between the SN Ib 1999dn at day −10 to the SN Ib Bmf4p41x4 model at day −16. However, this model spectrum is not well-matched since the He I features near 5650 Å and 6900 Å are significantly too red in wavelength. Increasing the overall kinetic energy for the model, among other variables, can resolve this discrepancy. However, the issue that remains is whether this increase would result in a 6250 Å feature that is too blue in wavelength. Even so, if a match is deemed secure for a model such as Bmf4p41x4, then this would imply the progenitor had $\sim 10^{-3}\,M_{\odot}$ of remaining hydrogen in its outermost layers, as a SN Ib.

Alternatively, James & Baron (2010) previously presented PHOENIX calculations to show that unburned hydrogen at high expansion velocities (in a shell) is reasonable for SN 1999dn (this comparison is also shown in Figure 4.) In this paradigm, the detachment velocity of the hydrogen shell is treated as a free parameter. With the shell displaced to 19,000 km s^{-1}, the material needed in the atmosphere of SN Ib 1999dn to reproduce the 6250 Å feature ($M_{\rm H} \lesssim 10^{-3}\,M_{\odot}$) is less than 0.01 $M_{\odot} < M_{\rm H} \lesssim 0.2\,M_{\odot}$ inferred for SN IIb 1993J by Baron et al. (1995). This mass estimate does not also conflict with the swept-up $5 \times 10^{-2}\,M_{\odot}$ estimated from model comparisons to late-nebular spectra of SN IIb (Jerkstrand et al. 2015).

3.2.3. SN Ib 2008D

Dessart et al. (2012) compared their Bmf5p09x4 model corresponding to 10.3 days since explosion to the February 2 spectrum of the SN Ib 2008D. In terms of the number of days since maximum light and with a rise-time of 36 days for the model, this corresponds to drawing a comparison between a model at day −26 and an observed event at day +4, a difference of one month.

In Figure 5 we compare the day −34 spectrum of Bmf5p09x4 (the earliest available) with the day −13, −15, and −17 observations of SN 2008D. Apart from the discordant epochs, the model spectrum does not confidently resemble those of SN 2008D prior to maximum light. The data are also fairly noisy at these early epochs. However, this particular model is not optimized for drawing conclusions on the validity of Si II λ6355 for SN 2008D.

If both computed and observed spectra were those of SN Ia, the differences are enough to signify different subtypes that may or may not be from the same family of progenitors. Specifically, and compared with SN Ia where detections of Si II have been verified, the earliest computed spectrum of

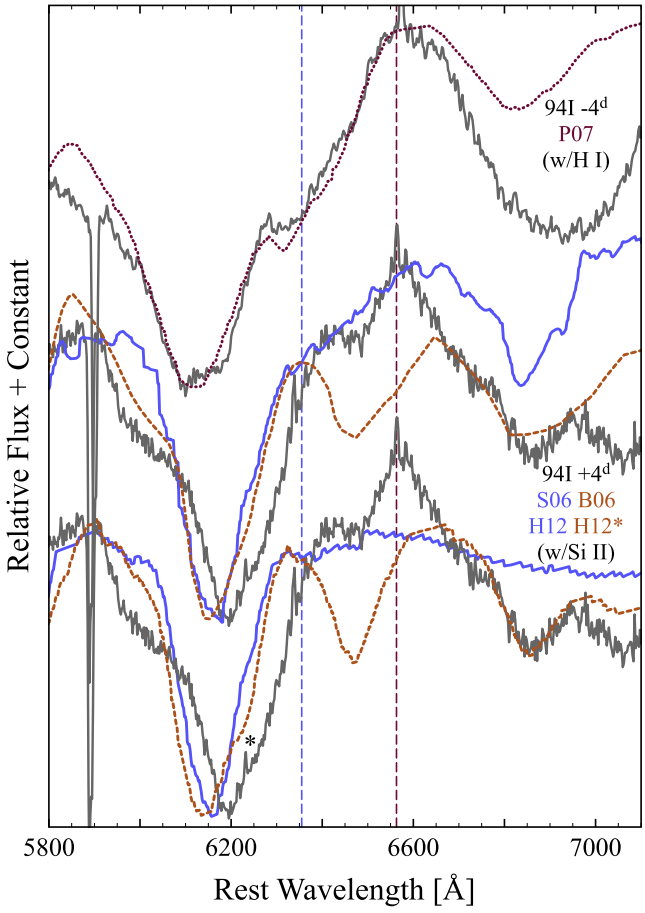

Figure 6. Model spectra compared with SN Ic 1994I (Modjaz et al. 2014). Model references: (P07) SYNOW calculation of Parrent et al. (2007) with hydrogen treated as a free parameter; S06 (Sauer et al. 2006); B06 (Branch et al. 2006); H12 models are from Hachinger et al. (2012). The blue model, H12, is the base SN Ic 94I model 16 days after explosion in the top of their Figure 11 in green. The orange model, H12*, corresponds to the hydrogen-enriched SN Ib in the top of their Figure 11 in red. The black asterisk is near the location of Hα coming through in this model. Like S06 and B06, both H12 models fail to match the minimum 6250 Å in SN Ic 1994I as they too are reliant on significant contribution from Si II λ6355. The vertical dashed lines denote the rest-wavelength of Si II λ6355 (blue) and H I λ6563 (red).

Bmf5p09x4 does not overlap the 6250 Å feature in the spectrum of SN 2008D near the date of explosion. One expects improvement through either a stronger contribution from Fe II or lower mean expansion velocities attributed to Si II, or the model is flawed ab initio.

3.2.4. "SN Ic" 1994I

For SN 1994I, a so-called "standard SN Ic," two opposing interpretations prevail in the literature for two models that produce mismatched signatures of Si II compared with observations (cf. Branch et al. 2006; Sauer et al. 2006). See Figure 6 where we have overplotted these two independent results.

Sauer et al. (2006) predict the feature centered about 6200 Å in the photospheric phase spectra of SN 1994I is primarily a product of C II, Ne I, and Si II, with mostly Si II present near maximum light. Based on their series of model spectra, including the fit near maximum light shown in Figure 6, Sauer et al. (2006) claim a satisfactory match has been made.

Branch et al. (2006) previously used SYNOW to show that a satisfactory solution can be obtained for SN 1994I near maximum light when He I, O I, Ca II, Ti II, and Fe II are assumed to form within similar strata of ejecta. When Branch et al. (2006) incorporate Si II into the SYNOW fit, the predicted offset of the feature dominated by Si II is nearly identical to that later found by Sauer et al. (2006). Thus, while it is reasonable to expect a multi-component prescription throughout the spectra of SN Ib/Ic, it is unreasonable to suspect a correct interpretation for over-prescribed C II, Ne I, and Si II when the model used to support this prescription is incapable of producing the complex evolution of the data (cf. Baron et al. 1999; Ketchum et al. 2008).

Hachinger et al. (2012) later used the model of Iwamoto et al. (1994) to argue that Si II λ6355 is a viable option for the 6250 Å feature in SN 1994I and that this signature of Si II can be contaminated by other species including Hα. However, despite offering to remedy the mismatch of model spectra with increased contribution from Hα, the hydrogen/helium-enriched C+O models of Hachinger et al. (2012) remain dominated by ill-matched Si II λ6355. See Figure 6 and note the asterisk next to the orange H12* spectrum near 6200 Å; this dip is the Hα coming through.

At the top of Figure 6 we have plotted the fit produced by Parrent et al. (2007) with SYNOW where the contribution from Hα was treated as a free parameter. It is important to reiterate that the assumptions of the SYNOW/SYNAPPS model are not realistic. Therefore, best guesses for a composition without any prior information from more detailed investigations cannot necessarily be considered superior on account of a well-matched output spectrum. However, the primary purpose of SYNOW-like tools is to quickly explore where detailed models are consistently unsuccessful.

To compare with the more recent "SN Ic" calculations of Dessart et al. (2015b), in Figure 5 we included timeseries observations of SN 1994I and overplotted the earliest computed spectrum of 5p11Ax1 at day −31 with the day +23 spectrum of SN 1994I. Overall, one can see that the match is promising. However, the early evolution of the 6250 Å feature observed for SN 1994I remains unaccounted for by the model. The 6250 Å feature at a particular epoch may be dominated by Si II and Fe II; however, there are no spectra of 5p11Ax1 prior to day −31 to conclude whether this is the case.

3.2.5. Other SN Ib/Ic

Plotted in Figure 7 are the spectra of several SN Ib, SN Ic, and SN Ib/Ic like events, e.g., SN 1984L, 1987M, and 2013ge (Drout et al. 2015). Similar to Figures 4 and 5, we have included comparisons to select model spectra from Dessart et al. (2012, 2015).

In the middle panel of Figure 7, we see the day −34 Bmf5p09x4 model spectrum from Dessart et al. (2012) is most comparable to the SN Ib 2004gq, yet the blueward offset in wavelength for the 6250 Å feature is evident. Events that are similar to SN 2004gq include SN Ib 2004fe, 2009iz, 2009jf, and 2006ep during pre-maximum epochs. For the SN Ib 1990I, the feature nearest to 6250 Å on its red-most side is likely blended with a signature of He I λ6678 and possibly with some contribution from C II.

For the spectrum of the SN Ib 1984L, a He I λ5876 feature centered about ∼5680 Å implies a mean projected Doppler velocity of 10,000 ± 500 km s^{-1}. Looking redward to the

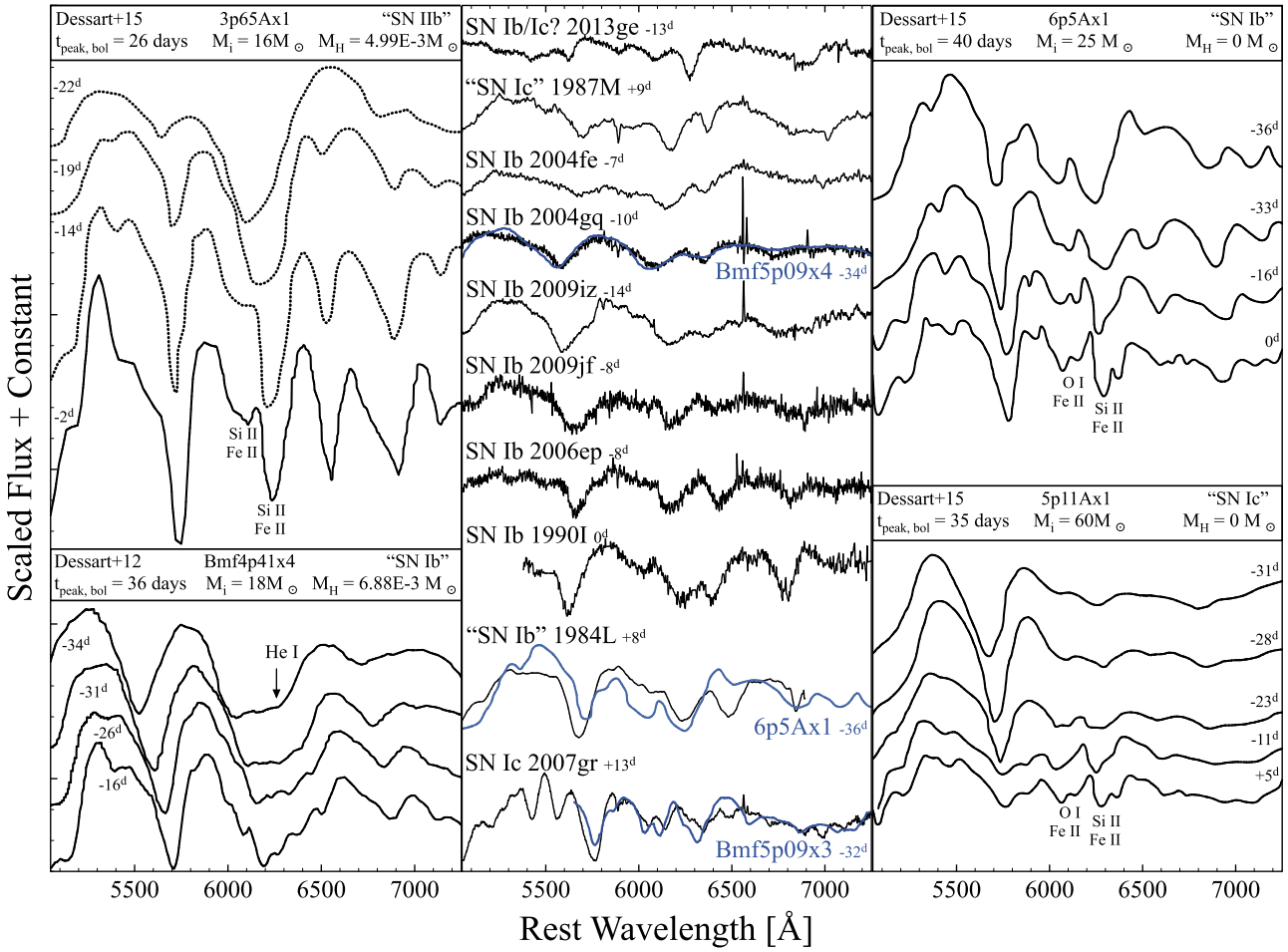

Figure 7. Same as Figure 4, except now for select SN Ib/Ic. Spectrum references: SN 1984L (Wheeler & Levreault 1985); SN 1987M (Filippenko et al. 1990; Jeffery et al. 1991); SN 1990I (Elmhamdi et al. 2004); 2004fe, 2004gq, SN 2006ge, SN 2007gr (telluric corrected), SN 2009iz, SN 2009jf (Modjaz et al. 2014, see also Valenti et al. 2011); and SN 2013ge (Drout et al. 2015).

feature centered about 6250 Å, associating the minimum with Si II λ6355 implies a mean projected Doppler velocity of $5000 \pm 500\,\mathrm{km\,s^{-1}}$. This differs from that inferred from He I by as much as $5000\,\mathrm{km\,s^{-1}}$. This suggests an association between Si II λ6355 and the minimum of the 6250 Å feature is unlikely.

Comparison between the day +8 spectrum of SN 1984L and the day −36 spectrum of the SN Ib 6p5Ax1 model from Dessart et al. (2015b) reveals moderate agreement. However, this particular benchmark model is not well-matched enough to invoke an unproven detection of Si II λ6355. Specifically, the projected Doppler velocities of the model and observations are not in sync. A visual comparison with the subsequent 6p5Ax1 model spectra (top right panel of Figure 7) does not also reveal a more accurate match; i.e., the relative strength of the He I signatures improve, but the projected Doppler velocities remain too low. We emphasize that the 6p5Ax1 model has not been built for SN 1984L, yet this model still does not provide accurate predictions for any SN Ib shown in Figure 7. This may be due in part to signatures of Si II λ6355 that are too strong for the model.

There does exist a fair visual agreement between the 6170 Å feature in the SN Ic 1987M and the $9000\,\mathrm{km\,s^{-1}}$ Si II profile produced by Dessart et al. (2012) for SN Ib 2008D; i.e., in our Figure 7 comparison with a computed profile of Si II is arguably convincing. However, a composition that is contaminated by trace hydrogen is difficult to rule out since the epoch of the only available spectrum (∼day +9) is not early enough to disaffirm tentative detections of weak signatures from hydrogen and helium atoms (Jeffery et al. 1991).

For the SN Ic 2007gr, which is plotted in Figures 7 and 8, Dessart et al. (2012) draw an association between the feature centered about 6350 Å as a composite of Si II on the blue wing forming with a line velocity of $\sim 6000\,\mathrm{km\,s^{-1}}$ and Fe II near the minimum and redward. For the full fit, the day −32 Bmf5p09x3 model spectrum at these wavelengths is promising when compared with the day +13 spectrum of SN 2007gr. However, given the overall blueward displacement of the model compared with observations, we interpret the corresponding line velocities as being too high.

Validation of this model for SN 2007gr could benefit, e.g., by a modest reduction of the kinetic energy released (this was done by Branch et al. 2002 who used SYNOW to interpret and measure Fe II lines in the SN Ic 1990B). However, the Si II would still remain too blue to confidently associate Si II with the absorption minimum of the 6350 Å feature. If the computed spectrum were well-centered about this 6350 Å feature, we suspect the absorption minima between the observed and

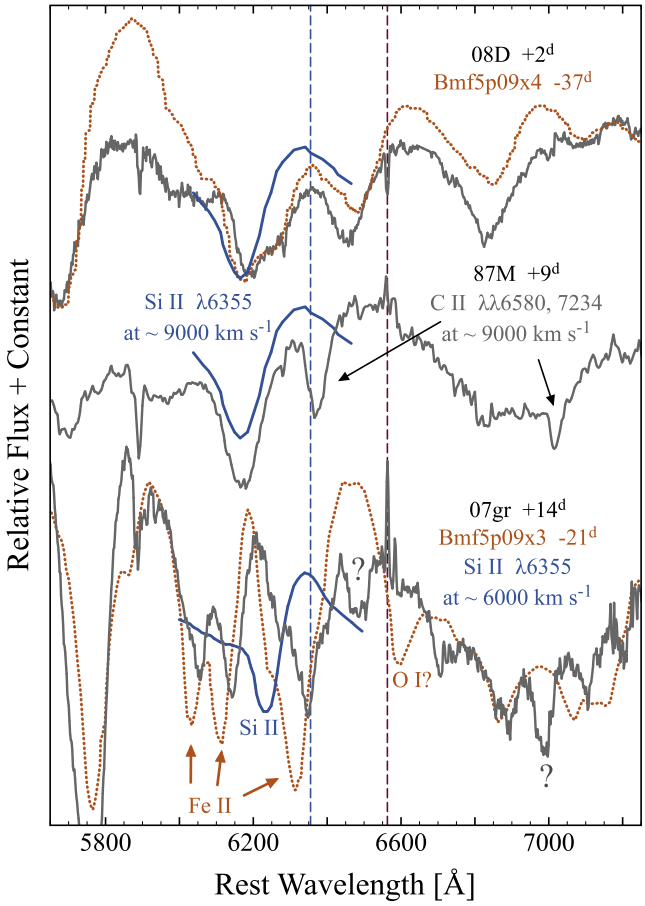

Figure 8. Model spectra from Dessart et al. (2012) (in orange) compared with the SN Ib 2008D and the SN Ic 2007gr. The blue Si II profiles computed for SN 2007gr and SN 2008D correspond to mean projected Doppler velocities of ~6000 km s^{-1} and 9000 km s^{-1}, respectively.

synthesized spectrum would be significantly offset at other wavelengths.

At the bottom of Figure 8 one can also see that the computed spectrum produces a Si II λ5972 feature that is not observed for SN 2007gr in this region, which is possibly contaminated by narrow Na I. In addition, there is less of a "Si II" notch on the blue wing of the larger 6350 Å feature to constrain the model when the observed spectrum is corrected for telluric features (cf. Modjaz et al. 2014). Subsequently, we find the detection of Si II λ6355 in SN 2007gr to be either unlikely and therefore not representative of "Si II features" of SN Ib/Ic in general, or that the contribution from Si II λ6355 is minimal for these kinds of core-collapse events.

3.3. Super-luminous Supernovae

The same distinctions used for classical types I and II are also used for SLSNe. SLSN II show conspicuous signatures of hydrogen; however, the hydrogen feature is so far like that of SN IIn (Dessart et al. 2015a), i.e., narrow emission signatures of hydrogen, e.g., SN 2006gy (Smith et al. 2007) and 2008am (Chatzopoulos et al. 2011).

For SLSN I, a spectral feature in the vicinity of 6000–6400 Å is either truly absent (or faint under noise) or a large and likely blended P Cygni profile is present. SLSN I spectra with a conspicuous 6250 Å feature, i.e., similar to those observed for SN 2007bi, LSQ12dlf, and iPTF13ehe, are frequently declared to be without a hydrogen feature or even so far as "hydrogen-free" (Gal-Yam et al. 2009; Nicholl et al. 2015; Yan et al. 2015).

However, recall from Figure 1 of Filippenko (1997) where the 6250 Å feature in SN Ib/Ic spectra has been imprecisely labeled to signify an identification of "weak Si II" despite a conflicting definition of no silicon detected within Section 2.1 of Filippenko (1997). Under the assumption that "type I means no hydrogen," an alternative interpretation of "weak Si II λ6355" is often applied to the relatively large 6250 Å P Cygni profile in the spectra of some SLSN I and all BL-Ic.

Hence, if SN Ib/Ic and SLSN I shared the same "weak silicon" feature, then perhaps one would expect to see other lines of Si II in the spectra of BL-Ic and SLSN I where the feature is much stronger. Thus far, however, no strong evidence favoring a detection of other lines of silicon, e.g., Si II λλ3858, 5972, has surfaced, while the low signal-to-noise ratios and low follow-up frequencies for these events prohibit more detailed investigations.

In the following subsections we focus our attention on Figure 9 where we have plotted comparisons between computed and observed spectra of BL-Ic and SLSN I that are found throughout the literature. Inconsistencies of models that produce signatures of Si II λ6355 are discussed in Section 3.3.1, and we again highlight spectral influence from Hα or ejecta contaminated by unburned hydrogen, as a promising alternative in Section 3.3.2.

3.3.1. Si II λ6355 as a Candidate Identification

Close inspection of Figure 9 reveals an insufficient match between models that produce strong signatures of Si II λ6355 and observations of BL-Ic and SLSN. A mismatch of "too blue" in wavelength is observed for a majority of these fully stripped C+O models from Iwamoto et al. (1994), and either without any improvement in subsequent adaptations to BL-Ic and SLSN or with the same conclusion of a model with a relatively shallower density profile compared with the observations.

For the BL-Ic 1998bw, the emission component produced by the model near 6500 Å is nearly 100 Å too blue to match observations without considerable absorption via ad hoc prescriptions of C II, Ne I, and Fe II. However, if the model were improved near 6200 Å with C II and Ne I, these ions would be at odds with the data at other wavelengths (cf. Elmhamdi et al. 2006, 2007). Alternatively, and using SYNAPPS, one could over-fit the region near 6300 Å with C II and Fe II to secure a plausible match. Ultimately, however, the fit would suffer at bluer wavelengths, as shown recently by Toy et al. (2015) for SN 2013dx, which is similarly associated with a gamma-ray burst event.

As for BL-Ic 2002ap (Foley et al. 2003), the 9000 km s^{-1} Si II profile from Dessart et al. (2012) reveals similar problems of "too blue" without an ad hoc prescription of adjacent species that are not immediately detected elsewhere. In particular, the discrepancy between the curvature of the computed profile dominated by Si II λ6355 and that from observations indicates that Si II λ6355 cannot be directly associated with the minimum of the 6250 Å feature in BL-Ic 1998bw and 2002ap. Similar conclusions apply to so-called "Hypernovae" such as SN 2003hd (Deng et al. 2005) and 2003lw (Mazzali et al. 2006). In addition, spectrum computed

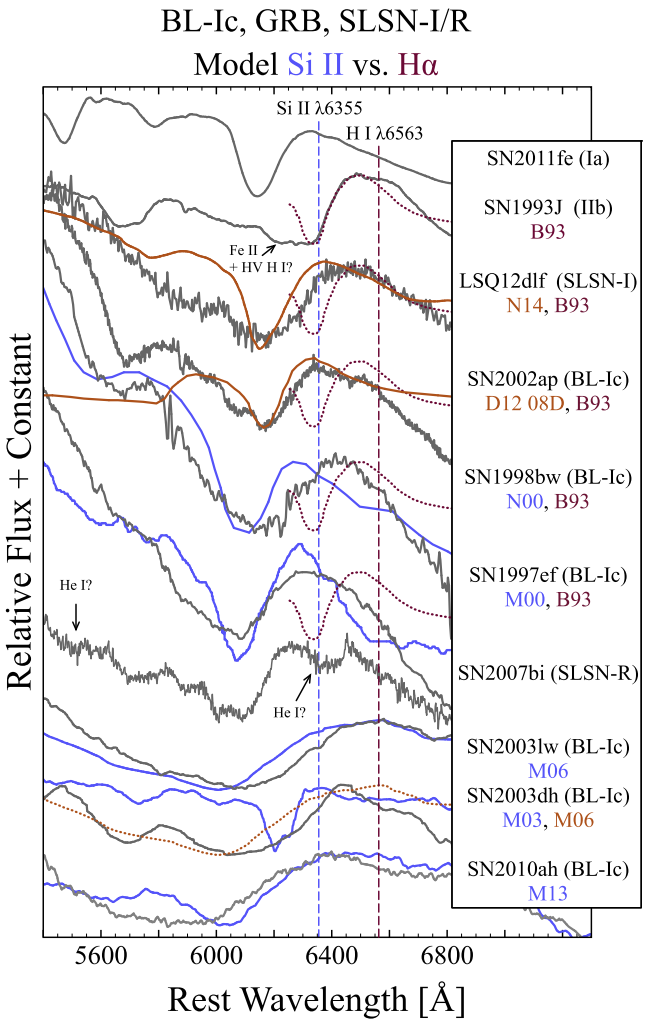

Figure 9. Comparisons between computed spectra and a selection of BL-Ic, SLSN, SN 1993J, and SN 2011fe. Spectrum references: SN 1993J (Barbon et al. 1995); SN 1997ef (Modjaz et al. 2014); SN 1998bw (Patat et al. 2001); SN 2002ap (Modjaz et al. 2014); SN 2003dh (Deng et al. 2005); SN 2003lw (Mazzali et al. 2006); SN 2007bi (Gal-Yam et al. 2009); SN 2010ah (Corsi et al. 2011); SN 2011fe (Pereira et al. 2013); and LSQ12dlf (Nicholl et al. 2015). Model references: (B93) Baron et al. (1993); (N00) Iwamoto et al. (1998); Nomoto et al. (2000); (M00) Mazzali et al. (2000); (M03) Mazzali et al. (2003); (M06) Mazzali et al. (2006); (D12 08D) Si II profile from a computed spectrum by Dessart et al. (2012), initially compared with SN Ib 2008D; (M13) Mazzali et al. (2013); and (N14) Nicholl et al. (2014).

for SN 2003dh conflicts with observations throughout, including wavelength regions not shown in our Figure 9.

Comparison between the the March 7 spectrum of SN 2010ah (PTF10bzf) and the computed spectrum of Mazzali et al. (2013) is shown at the bottom of Figure 9. For this BL-Ic, Mazzali et al. (2013) utilize rescaled CO138 models of Iwamoto et al. (1998) to interpret spectral signatures. Here again we see that the model does not provide adequate predictions. However, unlike previous comparisons with BL-Ic and SLSN, this is the first time in Figure 9 that we see a computed spectrum under-shoot the observed 6050 Å feature. There are at least two avenues for addressing the discrepancy between a profile dominated by Si II λ6355 and observations of SN 2010ah.

1. The blue wing of the 6150 Å feature in the model conflicts with the observations, and similar to what is seen for SN 1997ef, 1998bw, 2002ap, 2003dh, and LSQ12dlf. One could posit that the model predicts velocities that are not as high as the observations and that a simple scaling of kinetic energies or a shallower ejecta density profile would address the mismatch, thereby shifting the computed spectrum blueward. This is marginally true within the span of wavelengths plotted in Figure 9. However, such a correction for features near 6000–6400 Å would create an additional mismatch as already seen for Ca II and Fe II features at other wavelengths (shown in Figure 6 of Mazzali et al. 2013).
2. Alternatively, one could argue that the mismatch between the model spectrum does not correspond to the epoch needed for an appropriate comparison to SN 2010ah. However, had follow-up observations been obtained, i.e., for more than the two spectra obtained for SN 2010ah, we suspect the CO138 model spectrum would appear "too blue" near 6250 Å at an ostensibly appropriate epoch.

In Figure 9, the computed spectrum for the BL-Ic 1997ef (Mazzali et al. 2000) looks promising near the absorption minimum of the 6200 Å feature. However, viewed as a whole, it seems the parent models of CO21 (Iwamoto et al. 1994) and CO138H (Iwamoto et al. 1998) associated with the assortment of mismatched synthetic spectra are better suited for other supernovae yet to be observed.

The "type-R" SN 2007bi has been suggested to be powered by radioactive decay through pair instability (Gal-Yam et al. 2009). This origin, however, has since been contested (Moriya et al. 2010; Yoshida & Umeda 2011; Dessart et al. 2013; Chatzopoulos et al. 2015). Since a spectrum has not been computed for SN 2007bi, one can only guess at its composition by comparing SN 2007bi to other objects in Figure 9. Based on the similarity of 6000–6400 Å features, the 6250 Å feature for SN 2007bi is either not dominated by Si II, or the evidence favoring a detection of Si II is insufficient. A similarly fleeting "identification" of He I (indicated by the arrows in Figure 9) might instead favor either contamination from Hα near 6200 Å, or a composition that is not necessarily hydrogen-free.

Without sufficient improvements from stripped-envelope models that produce signatures of Si II λ6355, Nicholl et al. (2014, 2015) recently utilized SYNAPPS to identify Si II in the spectrum of another SLSN I, LSQ12dlf (shown near the top of Figure 9). The interpretation of Si II as the 6250 Å feature in LSQ12dlf is clearly inconsistent with the data from the red-most side of the emission component, through the absorption trough, and near the blue-most wing. Considering the observed feature slopes below the emission component of the proposed fit, which includes some Fe II, the mismatch is unavoidable without significant contribution from Fe II that, in the end, is difficult to constrain at other wavelengths. Moreover, and similarly for SN 2013dx (Toy et al. 2015), the spectrum of LSQ12dlf is too noisy to assess the underlying structure of the composite feature near 6250 Å.

Yan et al. (2015) recently presented observations of the SLSN I iPTF13ehe that revealed strong emission in Hα during late-nebular phases. Yan et al. (2015) conclude this CSM material originates from the progenitor in the years prior to the explosion and estimate a CSM mass of $\lesssim$30 $M_{\odot}$. Given that the progenitor masses for some of these SLSN I are thought to be 67–220 $M_{\odot}$, this would imply that the progenitor's mass is relatively high and possibly has trace amounts of hydrogen by

the time of the explosion. This of course depends on the episodes of mass loss throughout the progenitor's evolution.

Without providing a computed spectrum that is sufficiently matched to iPTF13ehe, Yan et al. (2015) also interpret the 6000–6400 Å feature as predominately Si II λ6355. Given the evidence for interaction between the ejecta of this SLSN I with material contaminated by hydrogen that was previously ejected (see also Chugai & Chevalier 2006; Milisavljevic et al. 2015), should we then expect trace amounts of hydrogen ($\sim 10^{-3}\ M_{\odot}$) to remain for massive stars, possibly as massive as $\sim 125\ M_{\odot}$?

More recently, Arcavi et al. (2014, 2015) presented observations of the rapidly rising PTF10iam. Arcavi et al. (2015) claim that the identification of its 6200 Å feature can be either Si II λ6355 or Hα. However, an interpretation of "either/or" is not applicable to unproven identifications of composite features.

Curiously, Arcavi et al. (2015) find a fair match between PTF10iam and the SN II 1999em, apart from SN II-like H-Balmer lines that are absent for PTF10iam. Arcavi et al. (2015) also compare the day +28 spectrum of PTF10iam to the day +11 spectrum of the SN Ia 1999ac, and claim that "the SN Ia fit is able to match this feature as Si II, as well as other features in the spectrum, with the major difference being that PTF10iam has additional broad hydrogen emission lines."

However, we find another major difference is that the 6200 Å feature in PTF10iam is not well-matched to the 6135 Å feature of SN 1999ac. In particular, the feature for SN 1999ac is noticeably too blue compared with that of PTF10iam. Furthermore, if the SN Ia 1999ac can be used to identify the 6200 Å feature of PTF10iam as Si II λ6355, while also "matching other features," why then is PTF10iam not classified as a SN Ia interacting with a H-rich medium?[3]

The spectra of PTF10iam are also noisy, and therefore do not have a well-defined minimum for the feature near 6200 Å (see also Greiner et al. 2015; Leloudas et al. 2015). However, for a 6200 Å feature to be identified as Si II λ6355, this corresponds to a line velocity of $\sim 8000\ \mathrm{km\ s^{-1}}$ ($\pm 1000\ \mathrm{km\ s^{-1}}$). For the SN Ia 1999ac spectrum that Arcavi et al. (2015) claim to have matched to PTFiam's 6200 Å feature, its Si II λ6355 line velocity is approximated to be $\sim 11{,}000\ \mathrm{km\ s^{-1}}$. Consequently, it is unlikely that the 6200 Å feature of PTF10iam can be solely attributed to Si II λ6355 and we suspect models that produce spectra dominated by Si II λ6355 will be unable to unequivocally match both the minimum and the blue and red wings of the 6200 Å feature without producing inconsistencies elsewhere.

This reliance on Si II λ6355 as a candidate identification reveals an ongoing problem. So far, there has been no observational precedent for lone signatures of Si II λ6355 outside of SN Ia (Wheeler et al. 1995; Filippenko 1997), nor has an accurate search of additional signatures of Si II been carried out. Yet the common wisdom for SN Ib, Ic, BL-Ic, and SLSN continues to default to a subjective and inconsistent identification of Si II λ6355. It is therefore a wonder why Si II λ6355 has been so strongly favored as an interpretation (cf. Figure 1 of Filippenko 1997 and Figure 2 of Modjaz et al. 2014). A more likely alternative identification is not necessarily Hα, much less Hα alone. Rather, a 6200 Å feature that is influenced by trace amounts of ejected hydrogen would be supported by the same observations of PTF10iam purportedly interacting with a H-rich medium near maximum light (Arcavi et al. 2015).

[3] PTF10iam is not likely a SN Ia because it does not look like a SN Ia prior to day +28. Yet an identification for its 6200 Å feature is being interpreted as Si II λ6355 based on an unmatched comparison to the SN Ia 1999ac, while an identification of Si II λ6355 is so far only definitely detected for SN Ia (Wheeler et al. 1995; Filippenko 1997).

3.3.2. H I λ6563 as a Candidate Identification

Compared with Hα in SN II spectra, SN IIb show weaker, albeit typical, signatures of hydrogen alongside conspicuous helium lines (Filippenko 1988). The Hα profile for SN IIb is also generally broader than that for SN II because the mass of the remaining hydrogen is greater for SN II than SN IIb. Consequently, the relative weakness of Hα in SN IIb spectra enables adjacent blending from species such as Si II, Fe II, and possibly higher velocity H I to broaden a spectral feature that would otherwise be solely attributed to Hα (Milisavljevic et al. 2013 and references therein).

Considering the similarity of all BL-Ic and select SLSN I/R plotted in Figure 9, we find contamination by Hα to be a plausible solution. One caveat is that the classically defined rest-wavelength P Cygni emission component of the observed feature is not centered about a rest-wavelength of 6563 Å. For SN II, Anderson et al. (2014) have shown the blueshifted emission of Hα is sensitive to the ejecta density profile, particularly when the radial falloff is steep. Blue-shifted emission components in Hα have also been observed for SN IIb, e.g., the well-observed SN 1993J (Baron et al. 1993). Therefore, another solution that would support an interpretation of hydrogen for BL-Ic and select SLSN I/R is if the underlying emission component of Hα is blueshifted along with the corresponding absorption minimum.

3.4. Measures of Projected Doppler Velocity

Estimates of so-called detachment velocities for hydrogen are either accurate from first principles, or direct measurements are again spoiled by effects of radiation transport in that the absorption minimum does not accurately estimate mean projected Doppler velocities for Hα (cf. Branch 1977). Under the assumption of either localized line formation, or multiple resonance line scattering (effectively SYNAPPS), line velocities inferred from absorption minima may overshoot the optimum position of these ostensibly found hydrogen-deficient regions of ejecta. If faint Hα in SN Ib, Ic, BL-Ic, and SLSN I/R behaves similarly compared with SN II and IIb, then trace amounts of detectable hydrogen would indicate high projected Doppler velocities in spite of being relatively closer to the photospheric line forming region (cf. Anderson et al. 2014).

By contrast, the redshift needed to rectify ill-matched signatures of Si II λ6355 is on the order of 200 Å. The effect that opposing interpretations of Si II λ6355 versus Hα has on estimates of line velocities is shown in Figure 10 for the SN Ib 2008D. Assuming one line dominates the 6250 Å feature, the error would be on the order of $\delta v \sim 9000\ \mathrm{km\ s^{-1}}$ between Si II λ6355 and Hα; i.e., noticeably large when spectroscopic resolutions of blended features are on the order of $\gtrsim 750\ \mathrm{km\ s^{-1}}$ for these classes of SN I. Compared with the SN Ia 2011fe, where signatures of both Si II Fe II can be used to trace respective line velocities, the same conclusion is not reached when considering the SN Ib 2008D.

Similarly, line velocities of Fe II are also noticeably higher than that of Si II λ6355 for SN 1994I, 1998bw, 2002ap,

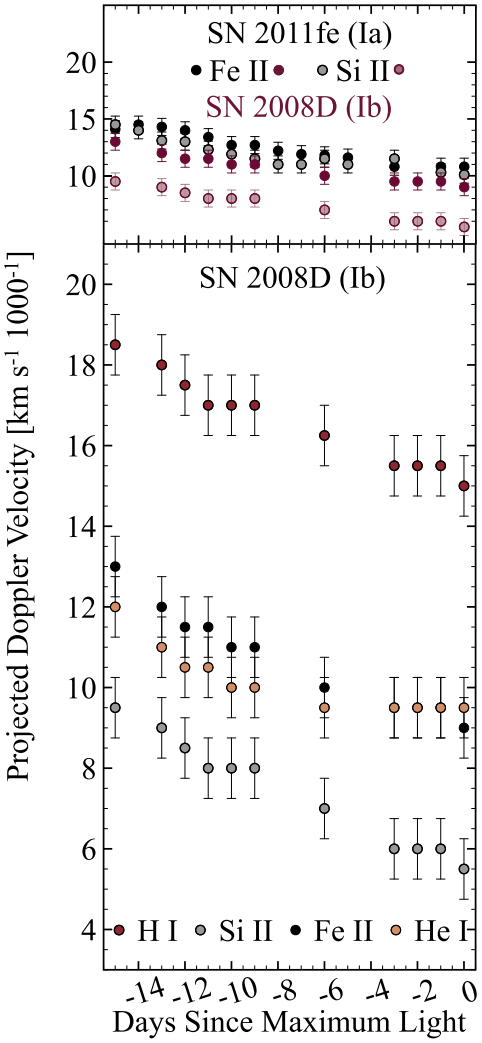

Figure 10. Estimated line velocities of SN Ib 2008D from its absorption minima. Vertical error bars shown for Si II and Fe II represent a minimum error of ±750 km s^{-1}. The errors could be as high as 2000 km s^{-1}. Shown above are values obtained for the SN Ia 2011fe using SYNAPPS (Parrent et al. 2012).

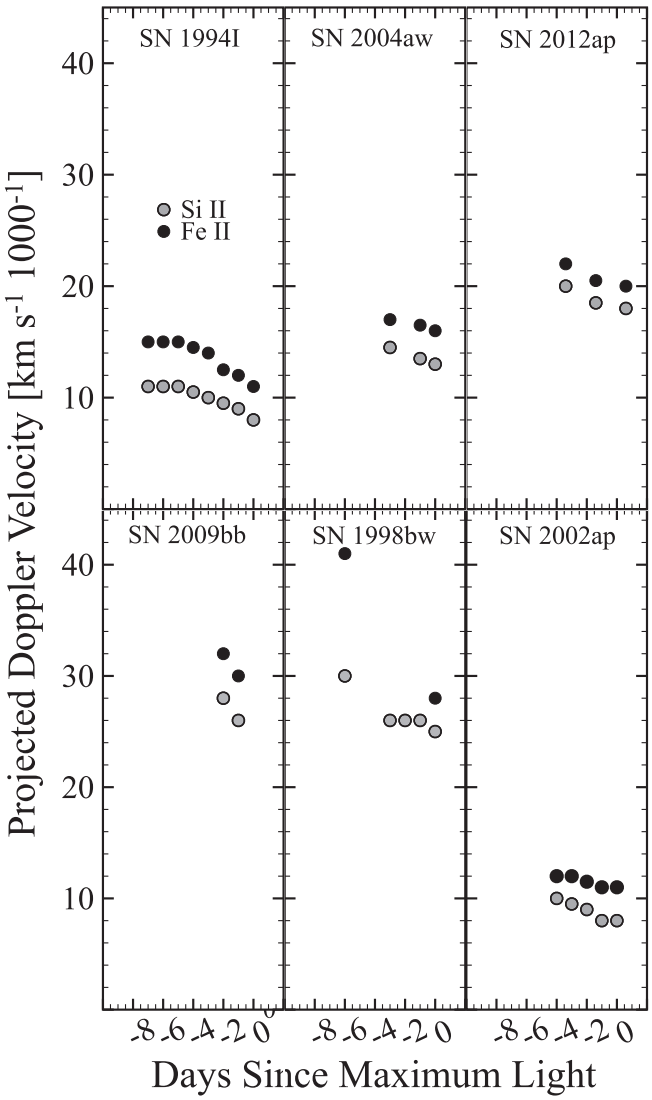

Figure 11. Estimated line velocities of 6000 Å features in SLSN and BL-Ic spectra. The gray points denote values obtained under an assumption that the absorption minimum is identified with Si II λ6355. Estimates of line velocities for Fe II are the points shown in black. For some of the available observations, we excluded points that did not have either an obvious minimum or underlying structure.

2004aw, 2009bb, and 2012ap, shown in Figure 11 (see also Table 2 of Stathakis et al. 2000). This trend continues into post-maximum epochs that are not shown, and indicates that if a signature of Si II λ6355 is shaping the spectrum, then it is weak and contributing to the blue-most wing of 6000 Å absorption features (instead of dominating an entire profile, much less the minimum).

4. SUMMARY AND CONCLUSIONS

In this work we examined publicly unavailable model spectra from both "hydrogen-poor" ($M_{\rm H} \sim 10^{-3}$–$10^{-2}\ M_{\odot}$) and "hydrogen-depleted" ($M_{\rm H} \sim 10^{-6}\ M_{\odot}$) compositions and compared them to observations of multiple SN I subclasses. Apart from natural uncertainties from line blending, and regardless of the spectrum synthesizer used, all one-dimensional model spectra intended for thermonuclear SN Ia are well-matched (Figure 3). Since the evidence favoring a detection of Si II λ6355 is overwhelming, direct association between Si II λ6355 and the minimum of 6150 Å features can be made in practice.

However for SN Ib, Ic, BL-Ic, and SLSN I/R, the evidence favoring detections of Si II λ6355 spans few events. This implies the direct association between Si II λ6355 and the minimum of 6000–6400 Å feature is not accurate. In addition, the observational evidence that would otherwise support an interpretation of Si II λ6355, e.g., signatures from lines other than λ6355, is as fleeting as any weak evidence that would similarly confirm the presence of trace hydrogen through Hβ (Figure 2).[4]

Among the available spectra stemming from models of stripped-envelope supernovae, and compared with observed 6000–6400 spectral features of SN Ib, Ic, BL-Ic, and SLSN, we find a consistent blueward mismatch in wavelength, in part due

[4] Although Section 2.1 of Filippenko (1997) claims Si II λ6355 is detected for SN Ia, but not for SN Ib/Ic, the labels of Si II λ6355 against SN Ia, Ib, and Ic spectra in Figure 1 of Filippenko (1997) are at odds with this statement. As a result, references made to this review have sided with either the labels of Figure 1 or the notions expressed within the body of the text.

to signatures of Si II λ6355 that are too strong. Subsequent explanations for this phenomenon have included a shallow density profile for the corresponding models (Hachinger et al. 2012 and references therein), or a prescription that is out of sync with the timeseries observations (see our Section 3.3.1). However, these notions are counter to both the successful interpretation of Si II for SN Ia (Figure 3), and the categorical shortcomings of stripped-envelope models that produce signatures of Si II that are too strong for pre-maximum observations of SN Ib, Ic, BL-Ic, and SLSN.

The inability of stripped-envelope models to accurately reproduce the shape of a given spectral feature could be attributed to many potential issues with velocities, composition, excitation/ionization, and assumptions of spherical symmetry in the model, and would not necessarily imply that a given model is fundamentally wrong (or right). However, if both photometry and timeseries spectra of a given event are to be thought of as sensitive to the radiation field and properties of the ejecta, then a model that is only approximately consistent with one of these pieces of information precludes firm conclusions about the nature of the spectral sequence being studied.

Contribution from species with line signatures near 6250 Å, such as C II and Fe II, may help to both prevent a poor match for a model and refine prescriptions for empirical measurements (cf. Dessart et al. 2015b). This solution, however, will require simultaneous agreement between the observed and computed photometry since this is so far not the case when an interpretation of Si II with Fe II has been put forward (see Section 3.2).

Furthermore, today's spectrum-limited observations do not provide the necessary constraints for invoking detections of C II through both λ6580 and λ7234 counterparts. This underscores the need for additional surveys that embark on maximizing follow-up frequency and signal-to-noise ratios throughout the evolution of the spectrum.

Among the most promising matches with stripped-envelope core-collapse models, two "realistic" model spectra can be described as being in fair agreement with two observations from two different objects; namely the hydrogen-poor ($M_{\rm H} \sim 10^{-3}\ M_{\odot}$) and compositionally mixed SN Ib model Bfm4p41x4 (Dessart et al. 2012) compared with the SN Ib 1999dn, and the hydrogen-depleted ($M_{\rm H} \sim 10^{-6}\ M_{\odot}$) SN Ib model Bmf5p09x4 (Dessart et al. 2012) compared with the SN Ib 2004gq. Even so, the rise-times for these models are not in good agreement with observations for these and most other SN Ib/Ic (cf. Wheeler et al. 2015), which brings into question the validity of the models altogether.

One might expect detailed modeling through PHOENIX and CMFGEN, both of which assume spherical symmetry for post-processing, to show some improvement at wavelengths redward of 6250 Å for hydrogen-depleted compositions since these synthesizers at least consider a larger volume of line formation than those methods that assume a sharp photosphere. However, such a redward fix does not appear to reveal itself in either the PHOENIX or CMFGEN synthetic spectra displayed in our Figures 4, 5, 7, and 8. In addition, an apparent absence of 200 Å line-shifts toward redder wavelengths for other spectral features appears to suggest that considerations of three-dimensional radiation transport would not conspire to enable the minimum of a Si II λ6355 profile to coincide with the observed minimum near 6250 Å.

Thus, an absence of faint Hα originating from trace hydrogen ($\sim 10^{-3}\ M_{\odot}$) is not simply a given for these SNe I, while the common wisdom has been to judge the quality of a computed spectrum from a fully stripped model by its [in] ability to match an unproven signature of Si II λ6355 within the feature centered about 6250 Å. Moreover, observations of would-be conspicuous signatures of hydrogen in the spectra of BL-Ic and SLSN I suggest that the broad emission component of Hα undergoes a significant blueward shift relative to the rest-wavelength of 6563 Å, which is an effect known to arise from steep density-gradients in the outermost ejecta of SN II in general (Baron et al. 1995; Anderson et al. 2014).

In the literature there are at least three promising models with computed spectra where $\sim 10^{-3}\ M_{\odot}$ of hydrogen is present within the outermost layers of ejecta, and the timeseries spectra for only one of these models is "Hα-negative." These include the SN IIb 3p65Ax1 (Dessart et al. 2015b), the aforementioned Hα-negative SN Ib Bmf4p41x4 (Dessart et al. 2012), and the calculations done by James & Baron (2010) who previously showed that Hα cannot be ruled out assuming extended regions of trace amounts of hydrogen for the SN Ib 1999dn. Hence, whether the computed spectrum for a hydrogen-poor event is Hα-positive, the mass of hydrogen in the outermost layers of some caught-early SN Ib, and therefore the progenitor, need not fall below $\sim 10^{-3}\ M_{\odot}$ for the model to remain consistent with 6250 Å spectral features (Section 3.2.1).

Depending on the sample of objects utilized to infer the progenitor and mass-loss history of "hydrogen-poor" supernovae (e.g., IIb/Ib), relationships may exist between properties of the light curves and the extent of trace hydrogen throughout the ejecta. Given a suite of improved model spectra, faint detections of Hα as well as non-detections stemming from trace hydrogen in the ejecta, might also be used to gain insights into the distribution of hydrogen near the surface of the progenitor star, or binary product, at the time of explosion.

This work was made possible by contributions to the Supernova Spectrum Archive (Richardson et al. 2001) and the Weizmann Interactive Supernova data REPository (WISeREP Yaron & Gal-Yam 2012), as well as David Bishop's Latest Supernovae page (Gal-Yam et al. 2013). This work has also made use of the Sternberg Astronomical Institute Supernova Light Curve Catalog, which is supported by grants of "Scientific Schools of Russia (3458.2010.2)," RFBR (10-02-00249).

All model spectra as well as most of the data that were not available on WISeREP at the time of our initial study were obtained with the help of the graph digitizer software, GraphClick.[5] (Digitizing one published spectrum of a supernova by hand takes about as long as it does to obtain the original spectrum with a CCD chip; ~20–50 minutes depending on the signal-to-noise ratio.)

J.T.P. is indebted to David Branch and J. Craig Wheeler for extensive discussions and valuable advice during the preparation of this manuscript. This work also benefitted from discussions with Rafaella Margutti, Maria Drout, Brian Friesen, Federica Bianco, and Isaac Shivvers, and additional comments from Gastón Folatelli.

Finally, we wish to thank our anonymous referee for taking the time to give constructive feedback.

[5] The full software is available at http://www.arizona-software.ch/graphclick/.

REFERENCES

Anderson, J. P., et al. 2014, MNRAS, 441, 671
Arcavi, I., et al. 2014, ApJ, 793, 38
Arcavi, I., et al. 2015, arXiv:1511.00704
Barbon, R., Benetti, S., Cappellaro, E., et al. 1995, A&AS, 110, 513
Baron, E., Branch, D., Hauschildt, P. H., Filippenko, A. V., & Kirshner, R. P. 1999, ApJ, 527, 739
Baron, E., Hauschildt, P. H., Branch, D., et al. 1993, ApJL, 416, L21
Baron, E., Hauschildt, P. H., & Mezzacappa, A. 1995, arXiv:astro-ph/9511081
Baron, E., Hauschildt, P. H., Nugent, P., & Branch, D. 1996, MNRAS, 283, 297
Benetti, S., et al. 2004, MNRAS, 348, 261
Blondin, S., Dessart, L., & Hillier, D. J. 2015, MNRAS, 448, 2766
Blondin, S., & Tonry, J. L. 2007, ApJ, 666, 1024
Branch, D. 1977, MNRAS, 179, 401
Branch, D., Baron, E., Hall, N., Melakayil, M., & Parrent, J. 2005, PASP, 117, 545
Branch, D., et al. 2002, ApJ, 566, 1005
Branch, D., et al. 2006, PASP, 118, 560
Chakraborti, S., Ray, A., Smith, R., et al. 2016, ApJ, 817, 22
Chatzopoulos, E., van Rossum, D. R., Craig, W. J., et al. 2015, ApJ, 799, 18
Chatzopoulos, E., et al. 2011, ApJ, 729, 143
Childress, M. J., et al. 2013, ApJ, 770, 29
Chugai, N. N., & Chevalier, R. A. 2006, ApJ, 641, 1051
Clocchiatti, A., Wheeler, J. C., Brotherton, M. S., et al. 1996, ApJ, 462, 462
Corsi, A., et al. 2011, ApJ, 741, 76
Deng, J., Tominaga, N., Mazzali, P. A., Maeda, K., & Nomoto, K. 2005, ApJ, 624, 898
Deng, J. S., Qiu, Y. L., Hu, J. Y., Hatano, K., & Branch, D. 2000, ApJ, 540, 452
Dessart, L., Audit, E., & Hillier, D. J. 2015a, MNRAS, 449, 4304
Dessart, L., Blondin, S., Hillier, D. J., & Khokhlov, A. 2014a, MNRAS, 441, 532
Dessart, L., Hillier, D. J., Blondin, S., & Khokhlov, A. 2014b, MNRAS, 439, 3114
Dessart, L., Hillier, D. J., Li, C., & Woosley, S. 2012, MNRAS, 424, 2139
Dessart, L., Hillier, D. J., Woosley, S., et al. 2015b, MNRAS, 453, 2189
Dessart, L., Waldman, R., Livne, E., Hillier, D. J., & Blondin, S. 2013, MNRAS, 428, 3227
Doggett, J. B., & Branch, D. 1985, AJ, 90, 2303
Doull, B. A., & Baron, E. 2011, PASP, 123, 765
Drout, M. R., et al. 2015, arXiv:1507.02694
Eldridge, J. J., Fraser, M., Smartt, S. J., Maund, J. R., & Crockett, R. M. 2013, MNRAS, 436, 774
Elmhamdi, A., Danziger, I. J., Branch, D., et al. 2006, A&A, 450, 305
Elmhamdi, A., Danziger, I. J., Branch, D., & Leibundgut, B. 2007, in AIP Conf. Ser. 924, The Multicolored Landscape of Compact Objects and Their Explosive Origins, ed. T. di Salvo et al. (Melville, NY: AIP), 277
Elmhamdi, A., Danziger, I. J., Cappellaro, E., et al. 2004, A&A, 426, 963
Faran, T., et al. 2014, MNRAS, 445, 554
Filippenko, A. V. 1988, PASAu, 7, 540
Filippenko, A. V. 1997, ARA&A, 35, 309
Filippenko, A. V., Porter, A. C., & Sargent, W. L. W. 1990, AJ, 100, 1575
Filippenko, A. V., et al. 1995, ApJL, 450, L11
Folatelli, G., et al. 2014, ApJ, 792, 7
Foley, R. J., et al. 2003, PASP, 115, 1220
Foley, R. J., et al. 2009, AJ, 138, 376
Friesen, B., Baron, E., Wisniewski, J. P., et al. 2014, ApJ, 792, 120
Fryer, C. L. (ed.) 2004, Stellar Collapse, Vol. 302 (Dordrecht: Kluwer)
Gall, E. E. E., Polshaw, J., Kotak, R., et al. 2015, A&A, 582, A3
Gal-Yam, A., Mazzali, P. A., Manulis, I., & Bishop, D. 2013, PASP, 125, 749
Gal-Yam, A., et al. 2009, Natur, 462, 624
Ganeshalingam, M., et al. 2012, ApJ, 751, 142
Gaposchkin, C. P. 1936, ApJ, 83, 245
Garnavich, P. M., et al. 2004, ApJ, 613, 1120
Gray, R. O., & Corbally, J. C. 2009, Stellar Spectral Classification (Princeton, NJ: Princeton Univ. Press)
Greiner, J., et al. 2015, Natur, 523, 189
Hachinger, S., Mazzali, P. A., Taubenberger, S., et al. 2012, MNRAS, 427, 2057
Hatano, K., Branch, D., Fisher, A., Millard, J., & Baron, E. 1999, ApJS, 121, 233
Hatano, K., Branch, D., Qiu, Y. L., et al. 2002, Natur, 7, 441
Hillier, D. J., & Dessart, L. 2012, MNRAS, 424, 252
Inserra, C., et al. 2013, ApJ, 770, 128
Iwamoto, K., Nomoto, K., Höflich, P., et al. 1994, ApJL, 437, L115
Iwamoto, K., et al. 1998, Natur, 395, 672
James, S., & Baron, E. 2010, ApJ, 718, 957
Jeffery, D. J., Branch, D., Filippenko, A. V., & Nomoto, K. 1991, ApJL, 377, L89
Jeffery, D. J., Ketchum, W., Branch, D., et al. 2007, ApJS, 171, 493
Jerkstrand, A., Ergon, M., Smartt, S. J., et al. 2015, A&A, 573, A12
Kerzendorf, W. E., & Sim, S. A. 2014, MNRAS, 440, 387
Ketchum, W., Baron, E., & Branch, D. 2008, ApJ, 674, 371
Kromer, M., et al. 2013, MNRAS, 429, 2287
Leloudas, G., et al. 2015, ApJL, 815, L10
Lentz, E. J., Baron, E., Branch, D., & Hauschildt, P. H. 2001, ApJ, 557, 266
Li, W., et al. 2003, PASP, 115, 453
Liu, Y.-Q., Modjaz, M., Bianco, F. B., & Graur, O. 2015, arXiv:1510.08049
Lyman, J. D., Bersier, D., James, P. A., et al. 2016, MNRAS, 457, 328
Maguire, K., et al. 2010, MNRAS, 404, 981
Marion, G. H., et al. 2013, ApJ, 777, 40
Matheson, T., Filippenko, A. V., Li, W., Leonard, D. C., & Shields, J. C. 2001, AJ, 121, 1648
Maund, J. R., et al. 2013, MNRAS, 433, L20
Mazzali, P. A., Iwamoto, K., & Nomoto, K. 2000, ApJ, 545, 407
Mazzali, P. A., Walker, E. S., Pian, E., et al. 2013, MNRAS, 432, 2463
Mazzali, P. A., et al. 2003, ApJL, 599, L95
Mazzali, P. A., et al. 2006, ApJ, 645, 1323
Mazzali, P. A., et al. 2014, MNRAS, 439, 1959
Milisavljevic, D., et al. 2013, ApJ, 767, 71
Milisavljevic, D., et al. 2015, ApJ, 815, 120
Minkowski, R. 1941, PASP, 53, 224
Modjaz, M., et al. 2009, ApJ, 702, 226
Modjaz, M., et al. 2014, AJ, 147, 99
Moriya, T., Tominaga, N., Tanaka, M., Maeda, K., & Nomoto, K. 2010, ApJL, 717, L83
Moriya, T. J., Liu, Z.-W., Mackey, J., Chen, T.-W., & Langer, N. 2015, A&A, 584, L5
Nicholl, M., et al. 2014, MNRAS, 444, 2096
Nicholl, M., et al. 2015, MNRAS, 452, 3869
Nomoto, K., et al. 2000, in AIP Conf. Ser. 526, Gamma-ray Bursts, 5th Huntsville Symp., ed. R. M. Kippen, R. S. Mallozzi, & G. J. Fishman (Melville, NY: AIP), 622
Parrent, J., Friesen, B., & Parthasarathy, M. 2014, ApSS, 351, 1
Parrent, J., et al. 2007, PASP, 119, 135
Parrent, J. T., et al. 2011, ApJ, 732, 30
Parrent, J. T., et al. 2012, ApJL, 752, L26
Patat, F., Benetti, S., Cappellaro, E., et al. 1996, MNRAS, 278, 111
Patat, F., et al. 2001, ApJ, 555, 900
Pejcha, O., & Prieto, J. L. 2015, ApJ, 806, 225
Pereira, R., et al. 2013, A&A, 554, A27
Popper, D. M. 1937, PASP, 49, 283
Pun, C. S. J., et al. 1995, ApJS, 99, 223
Richardson, D., Thomas, R. C., Casebeer, D., et al. 2001, BAAS, 33, 1428
Sanders, N. E., Soderberg, A. M., Gezari, S., et al. 2015, ApJ, 799, 208
Sasdelli, M., Mazzali, P. A., Pian, E., et al. 2014, MNRAS, 445, 711
Sauer, D. N., Hoffmann, T. L., & Pauldrach, A. W. A. 2006, A&A, 459, 229
Smith, N., et al. 2007, ApJ, 666, 1116
Soderberg, A. M., et al. 2008, Natur, 453, 469
Stathakis, R. A., et al. 2000, MNRAS, 314, 807
Stritzinger, M. D., et al. 2014, A&A, 561, A146
Taubenberger, S., et al. 2006, MNRAS, 371, 1459
Taubenberger, S., et al. 2011, MNRAS, 412, 2735
Toy, V. L., et al. 2015, arXiv:1508.00575
Tsvetkov, D. Y. 1987, SvAL, 13, 376
Vacca, W. D., et al. 2015, ApJ, 804, 66
Valenti, S., et al. 2011, MNRAS, 416, 3138
Wheeler, J. C., Harkness, R. P., Clocchiatti, A., et al. 1994, ApJL, 436, L135
Wheeler, J. C., Harkness, R. P., Khokhlov, A. M., & Hoeflich, P. 1995, PhR, 256, 211
Wheeler, J. C., Johnson, V., & Clocchiatti, A. 2015, MNRAS, 450, 1295
Wheeler, J. C., & Levreault, R. 1985, ApJL, 294, L17
White, C. J., et al. 2015, ApJ, 799, 52
Yan, L., et al. 2015, ApJ, 814, 108
Yaron, O., & Gal-Yam, A. 2012, PASP, 124, 668
Yoshida, T., & Umeda, H. 2011, MNRAS, 412, L78